ETH
Eidgenössische Technische Hochschule Zürich
Swiss Federal Institute of Technology Zurich

Semester Thesis

Simulation and characterization of waveguides and the coupling to 3D microwave cavities

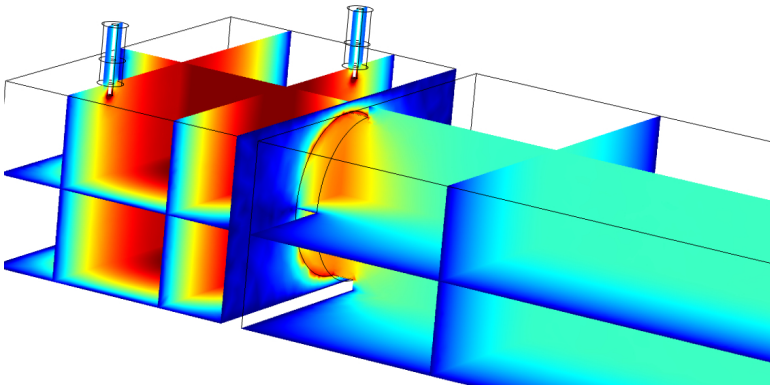

Silvia Ruffieux

Supervisor: Philipp Kurpiers
Professor: Prof. Dr. Andreas Wallraff
Quantum Device Lab

April 8, 2014

Abstract

A waveguide is a good option for a quantum channel with low transmission loss over a distance of 10 m as required in loop-hole free Bell-tests. In this semester thesis the transmission and coupling properties of waveguides are investigated. The WR90 and WR137 rectangular waveguide are chosen and simulations carried out using their dimensions. A first set of simulations studies the impact of various defects on the transmission through the waveguide. Tables for each defect show the effect on the S21 parameter for different sizes of the defect. The second set of simulations analyzes the coupling from a coaxial cable into a 3D microwave cavity. By varying the position of the coaxial cable on one side of the cavity, the length of the inner conductor protruding from the dielectric and the position of the dielectric, the coupling can be engineered as desired. The last set of simulations adds the waveguide to the model of the cavity and investigates the coupling through a circular aperture.

Contents

1 Motivation

One of the fundamental question of modern physics is if quantum mechanics can be reproduced by a local realistic theory. In a *local* theory the outcome of the measurement of one of two space-like separated particles does not influence the other particle directly. All measurements in a *realistic* theory have a pre-existing, yet unknown outcome. This outcome is for example determined by hidden variables. If one of these two conditions is not fulfilled, then quantum mechanics is not a local realistic theory, which sets quantum mechanics aside from classical physics.
An experimental test of Bell inequalities determines whether a theory is local realistic or not. Previously, a number of experiments have shown a violation of Bell inequalities indicating that quantum mechanics is not local realistic [1]. These measurements however contained loop-holes that have to be closed in order to exclude the possibility of a hidden variable theory. Two conditions have to be fulfilled in order to close the two loop-holes:

- Signaling loop-hole: the time to measure the two space-like separated particles has to be less than the time information requires to travel at the speed of light between the two particles.
- Detection loop-hole: The fraction of detected entangled pairs has to be above a certain threshold.

The signaling loop-hole was closed in experiments at optical frequencies in 1998 [10], while the detection loop-hole was closed using superconducting circuits [2]. So far no experiment was performed which closes both loop-holes simultaneously.
The goal of the "SuperQuNet" project is to close both loop-holes simultaneously. This should be done by separating two qubits by a suffient distance d and connecting them via a quantum channel to entangle them. In order to close the signaling loop-hole the distance d has to be longer than the distance light travels in the required measurement time. This results in a channel of about 10 m length. Since entanglement should be generated deterministically, the loss in the channel should be as low as possible. Waveguides show good properties as transmission lines because they show low loss over the intended distance. In this semester thesis waveguides as a transmission channel are investigated.

2 Theory of waveguides

2.1 Rectangular waveguides

A schematic of a rectangular waveguide is given in Figure 1. By convention the longer side a is along the x-axis and the shorter side b along the y-axis. The waveguide is filled with a material with permeability μ and permittivity ϵ.

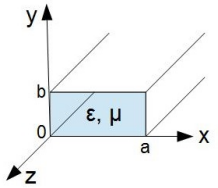

Figure 1: *Schematic of a rectangular waveguide with dimensions a and b filled with a material with permeability μ and permittivity ϵ.*

The propagating waves have to fulfill Maxwell's equations. In this case that means that the divergence of the electric field has to be zero, as there is no source of the electric field inside the waveguide. Close to the conductor surface, two rules have to be fulfilled: the electric field has to be orthogonal to the conductor and the magnetic field has to be parallel to the conductor. In TEM (transverse electro magnetic) waves, where both the electric and the magnetic field are orthogonal to the propagation direction, these conditions can only be fulfilled by the trivial solution, whereas the TE (transverse electric) and TM (transverse magnetic) modes can propagate. The detailed description of how Maxwell's equations are solved can be found in Pozar, chapter 3.1 and 3.3 [8]. The general assumptions are that the electric and the magnetic field in z-direction have a $e^{-i\beta z}$ dependance (β is the propagation constant) and that the waveguide region is source free. This reduces Maxwell's equations to 6 coupled differential equations for the 3 components of the electric field (E_x, E_y, E_z) and the 3 components of the magnetic field (H_x, H_y, H_z). These equations can be solved for the transverse field components. In that process the cutoff wave number k_c is defined as

$$k_c^2 = k^2 - \beta^2, \tag{1}$$

where k is the wave number of the material filling the waveguide:

$$k = \omega\sqrt{\mu\epsilon} = 2\pi f\sqrt{\mu\epsilon} = \frac{2\pi}{\lambda}. \tag{2}$$

As usually, ω is the angular frequency, f the frequency and λ the wavelength of the propagating wave.
For the electric and magnetic field along the direction of propagation, the Helmholtz wave equation has to be solved. Here we distinguish between the TE and TM modes.

TE modes have the electric field orthogonal to the propagation direction along the z-axis, so $E_z = 0$. Solving the Helmholtz equation leads to

$$H_z(x, y, z) = A_{mn} \cos\left(\frac{m\pi x}{a}\right) \cos\left(\frac{n\pi y}{b}\right) e^{-i\beta z}, \tag{3}$$

where A_{mn} is the amplitude constant. The indices m and n number the different modes, which appear due to the boundary conditions concerning the electric and magnetic fields close to the conductor surface mentioned above. The propagation constant β also depends on the indices m and n:

$$\beta = \sqrt{k^2 - k_c^2} = \sqrt{k^2 - \left(\frac{m\pi}{a}\right)^2 - \left(\frac{n\pi}{b}\right)^2}. \tag{4}$$

The propagation constant has to be real to correspond to a propagating mode, meaning that k has to be bigger than k_c. Modes that do not fulfill this condition are called cutoff modes or evanescent modes. These waves with an imaginary β decay exponentially away from the source of excitations. The wave number k is directly related to the frequency f by equation (2) and therefore a cutoff frequency $f_{c_{mn}}$ can be defined for each mode above which the mode can propagate:

$$f_{c_{mn}} = \frac{k_c}{2\pi\sqrt{\mu\epsilon}} = \frac{1}{2\pi\sqrt{\mu\epsilon}} \sqrt{\left(\frac{m\pi}{a}\right)^2 + \left(\frac{n\pi}{b}\right)^2}. \tag{5}$$

The lowest cutoff frequency is obtained for the so called dominant mode, which for rectangular waveguides is the TE_{10} mode with m = 1 and n = 0 resulting in

$$f_{c_{10}} = \frac{1}{2a\sqrt{\mu\epsilon}}. \tag{6}$$

There is no TE_{00} mode as all the electric field components would be zero. For a hollow waveguide $\frac{1}{\sqrt{\mu\epsilon}}$ is equal to the speed of light c in vacuum.
By choosing the dimensions a and b, the modes that can propagate in the waveguide can be chosen. The waveguide is called overmoded if there is more than one mode propagating at the selected frequency.

In waveguides attenuation may occur due to the finite conductivity of the material and dielectric loss. The second is neglectable if a waveguide is filled with air. Therefore, the dominant loss is due to the finite conductivity. In Pozar, chapter 3.3 [8], the attenuation α_c due to conductor loss is calculated for the TE_{10} mode:

$$\alpha_c = 8.686 \left(\frac{2\pi^2 R_s}{a^3 \beta k \eta} + \frac{k R_s}{b \beta \eta} \right) \quad \text{dB/m.} \tag{7}$$

The first factor comes from the conversion from nepers to decibels. The wall surface resistance R_s is related to the skin depth δ and is given by

$$R_s = \frac{1}{\sigma \delta} = \sqrt{\frac{\omega \mu}{2\sigma}}. \tag{8}$$

The square root of the ratio between the permeability μ and the permittivity ϵ is labeled with η:

$$\eta = \sqrt{\frac{\mu}{\epsilon}}. \tag{9}$$

Equation (7) implies that the loss at a given frequency is lower for larger waveguide dimensions a and b. The waveguide dimensions however also affect the modes being propagated.

TM modes have the magnetic field orthogonal to the propagation direction along the z-axis, so $H_z = 0$. This time the electric field component in propagation direction has to fulfill the Helmholtz equation leading to

$$E_z(x, y, z) = B_{mn} \sin\left(\frac{m\pi x}{a}\right) \sin\left(\frac{n\pi y}{b}\right) e^{-i\beta z}. \tag{10}$$

The calculation is very similar to the one for the TE modes and leads to the same propagation constant β as in equation (4). The TM_{mn} modes also have the same cutoff frequencies as in equation (5). The difference is that there are no TM modes with either m or n identically to zero as then the electric field in propagation direction would also be zero according to equation (10). Therefore there is no TM_{00}, TM_{10} and TM_{01} mode. The lowest propagating TM mode is the TM_{11} mode with a cutoff frequency of

$$f_{c_{11}} = \frac{1}{2\pi\sqrt{\mu\epsilon}} \sqrt{\left(\frac{\pi}{a}\right)^2 + \left(\frac{\pi}{b}\right)^2}, \tag{11}$$

which is higher than the cutoff frequency of the TE_{10} mode. Thus the dominant mode of the rectangular waveguide is the TE_{10} mode.

2.2 Circular waveguides

A rectangular shape is not the only possible geometry which supports the propagation of TE and TM modes. These modes can also propagate in circular waveguides, which is shown in the schematic in Figure 2. In general waveguides can be filled with a dielectric material with permeability μ and permittivity ϵ.

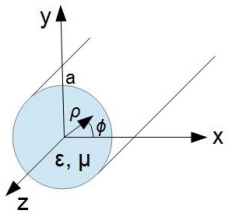

Figure 2: *Schematic of a cylindrical waveguide with radius a filled with a material with permittivity ϵ and permeability μ. Cylindrical coordinates with the variables ρ and ϕ are used.*

For cylindrical waveguides Maxwell's equations have to be solved in cylindrical coordinates. Same as for the rectangular waveguides, the assumption is made that the propagation in z direction is proportional to $e^{-i\beta z}$. A detailed calculation can be found in Pozar, chapter 3.4 [8]. Here only the main results will be given.
Waves with frequencies below the cutoff frequency f_c are damped exponentially. This time the cutoff frequencies have different expressions for TE and TM modes. For the TE modes the cutoff frequency is

$$f_{c_{mn}} = \frac{p'_{mn}}{2\pi a\sqrt{\mu\epsilon}}, \tag{12}$$

where p'_{mn} labels the nth root of the derivative of the Bessel function J_m. The cutoff frequency for the TM modes contains the nth root of the Bessel function J_m labeled with p_{mn} instead of the derivative:

$$f_{c_{mn}} = \frac{p_{mn}}{2\pi a\sqrt{\mu\epsilon}}. \tag{13}$$

The roots of the Bessel function and its derivative can be found in tables like in Ref. [3]. The most important are $p'_{11} = 1.841$ and $p_{01} = 2.405$.
The TE_{11} mode is the dominant mode of a circular waveguide. There is no TE_{10}, but there is a TE_{01} mode. The first TM mode is the TM_{01} mode.

The attenuation coefficient due to finite conductivity for TE modes can be found in Ref. [3]:

$$\alpha_{c_{mn}}^{\mathrm{TE}} = \underbrace{8.686 \frac{R_s}{a\eta\sqrt{1-\left(\frac{\nu_c}{\nu}\right)^2}}}_{\alpha_{c_{mn}}^{\mathrm{TM}}} \left(\left(\frac{\nu_c}{\nu}\right)^2 + \frac{m^2}{{p'_{mn}}^2 - m^2}\right) \quad \mathrm{dB/m}. \tag{14}$$

The first half of the formula is the attenuation coefficient for the TM mode. The wall surface resistance R_s (see equation (8)) and η (see equation (9)) are given in the section on rectangular waveguides.
The TE_{0n} modes received considerable attention because their attenuation constant decreases monotonically as a function of frequency. These modes are called the *circular electric modes* as the field lines of the electric field are all arranged in circles. The only tangential part of the field is the magnetic field in z-direction leading to the TE_{0n} having very low loss due to finite conductivity. The problem is that the TE_{01} mode is not the dominant mode. This means that other modes with lower cutoff frequencies and higher loss coexist with the TE_{01} mode. If there is more than one mode propagating, the signal is distorted, because each of the modes has a different attenuation coefficient and velocity. Defects in the geometry, the surface and the direction (e.g. bends) lead to coupling into other modes and make it hard to excite the TE_{01} mode with high enough purity.

2.3 Selected waveguides

The main advantage of the circular waveguide would be that the loss for the TE_{0n} modes goes to zero for high frequencies, but we can not make use of this property as it is accompanied by more than one mode being excited. We use the waveguides at frequencies where we only couple into the dominant mode to get an undistorted signal. For this mode the attenuation is of the same order of magnitude for rectangular and circular waveguides. For rectangular waveguides there are standard dimensions. Usually the ratio a:b is chosen to be 2:1. The loss goes to infinity at the lower cutoff frequency and therefore the generally accepted frequency range lays between 125% and 189% of the lowest cutoff frequency [9]. The commercially available rectangular waveguides cover a frequency range from 0.32 GHz (WR2300) to 1100 GHz (WR1). Two different types of rectangular waveguides are chosen for this project due to their frequency range: WR90 and WR137. The number stands for the longer length a of the cross section in hundredth of an inch. The characterizing data can be found in Table 1 [7].

	WR90	WR137
dimensions a x b in inches	0.90 x 0.40	1.372 x 0.622
dimensions a x b in mm	22.86 x 10.16	34.849 x 15.799
frequency range	8.20-12.4 GHz	5.85-8.20 GHz
cutoff frequency of the lowest mode	6.557 GHz	4.301 GHz
cutoff frequency of the next mode	13.114 GHz	8.603 GHz

Table 1: *Data of waveguides WR90 and WR137*

2.4 Measuring loss

Loss can be measured in different ways. An important quantity of transmission lines is the standing wave ratio (SWR) defined as

$$\text{SWR} = \frac{V_{max}}{V_{min}}. \tag{15}$$

It describes how well the load is matched to the transmission line. If the load is matched to the line (SWR = 1), the magnitude of the voltage is constant on the line. If the load is mismatched (SWR > 1), not all of the available power from the generator is delivered to the load. Some of the wave is reflected and a standing wave is obtained.
Another possibility is to measure the scattering parameters (S-parameters). S_{ij} is the power transmission coefficient P_i/P_j from port j to port i where all other ports are terminated in matched loads to avoid reflections. Usually the transmission is measured in decibels (dB). This unit compares two power levels P_1 and P_2:

$$10 \cdot \log_{10}\left(\frac{P_1}{P_2}\right) \quad \text{dB}. \tag{16}$$

Equal power levels lead to 0 dB, half the power level to -3 dB. Sometimes also nepers (Np) are used. This unit is defined with the voltage ratio and uses the natural logarithm instead of the decadic logarithm. 1 Np corresponds to 8.686 dB.
For resonators the quality factor Q can be found in two-port measurements [8]. When plotting the power transmission coefficient S_{21} as a function of frequency, a Lorentzian lineshape is obtained as plotted in Figure 3. A Lorentzian function is defined by the amplitude T_0, the resonance frequency f_0 and the bandwidth δf (FWHM) and is given by the function

$$F_{Lor} = \frac{T_0}{4Q^2} \frac{1}{\left(\frac{f}{f_0} - 1\right)^2 + \frac{1}{4}\frac{1}{Q^2}}. \tag{17}$$

The quality factor Q is defined as

$$Q = \frac{f_0}{\delta f}. \tag{18}$$

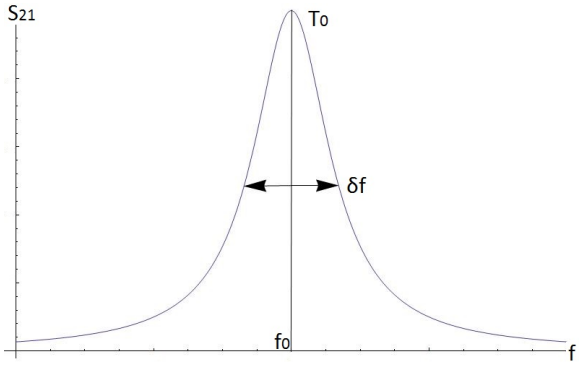

Figure 3: *Lorentz function with its defining variables the amplitude T_0, the bandwidth δf and the resonance frequency f_0.*

In general, it is not possible to measure the internal quality factor of a resonator directly, because of the loading effect of the measurement system. We therefore have to distinguish between different quality factors - the internal quality factor Q_{int} of the resonator and the coupling to the measurement systems corresponding to an external quality factor Q_{ext}. The loaded quality factor Q_L is measured directly and can be extracted by a Lorentzian fit of the S_{21} parameter measured versus frequency. The quality factors are related by

$$\frac{1}{Q_L} = \frac{1}{Q_{int}} + \frac{1}{Q_{ext}}. \tag{19}$$

The ratio $g = \frac{Q_{int}}{Q_{ext}}$ is called the coupling coefficient. The resonator is said to be

- overcoupled if $g \gg 1 \Rightarrow Q_L \approx Q_{ext}$,
- critically coupled if $g = 1$ and
- undercoupled if $g \ll 1 \Rightarrow Q_L \approx Q_{int}$ [5].

The internal and external quality factor can also be extracted by the Lorentzian fit if the measuring system has been calibrated correctly. The coupling con-

stant in a series RLC circuit is given by[1]:

$$g = \frac{\sqrt{S_{21}(f_0)}}{1 - \sqrt{S_{21}(f_0)}}, \tag{20}$$

which is derived in Pozar, chapter 6 [8]. The amplitude T_0 of the Lorentzian function corresponds to $S_{21}(f_0)$. With the coupling constant g a relation between the loaded and the internal quality factor can be obtained using equation (19):

$$\frac{1}{Q_L} = \frac{1}{Q_{int}} + \frac{1}{Q_{ext}} = \frac{1}{Q_{int}}\left(1 + \frac{Q_{int}}{Q_{ext}}\right) = \frac{1}{Q_{int}}(1+g) \tag{21}$$

This leads to an internal quality factor of

$$Q_{int} = Q_L(1+g) \overset{(20)}{=} Q_L\left(1 + \frac{\sqrt{T_0}}{1-\sqrt{T_0}}\right) = \frac{Q_L}{1-\sqrt{T_0}} \tag{22}$$

and using the definition of the coupling coefficient to an external quality factor of

$$Q_{ext} = \frac{Q_{int}}{g} = \frac{Q_L}{\sqrt{T_0}}. \tag{23}$$

The coupling from outside into a resonator can be assessed with the external coupling coefficient $\frac{\kappa_{ext}}{2\pi}$ which is defined as

$$\frac{\kappa_{ext}}{2\pi} = \frac{f_0}{Q_{ext}}. \tag{24}$$

The denominator 2π is used to express the external coupling coefficent in the units of a frequency instead of an angular frequency. The inverse of the coupling coefficient stands for the time a photon needs to transfer into the resonator. The bigger the external coupling coefficient, the stronger the coupling and the faster a photon is transferred into the cavity.

[1]The square root is required due to our definition of S_{21} as the ratio of the transmitted power instead of the voltage ratio. Power and voltage are related via $P = U^2/R$, which leads to the square root.

2.5 Rectangular waveguide cavity resonators

A 3 dimensional cavity can be constructed from closed sections of waveguides. This cavity has the dimensions a and b of the waveguide and the length d as can be seen in Figure 4.

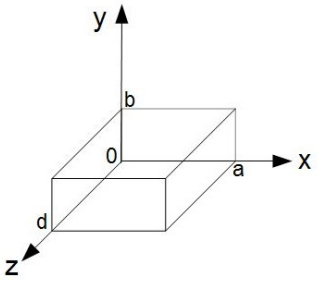

Figure 4: *Schematic of a rectangular waveguide cavity resonator with width a, height b and lenght d.*

In comparison to the waveguide the cavity is short circuited at both ends and therefore the boundary condition changes at the walls at $z = 0$ and $z = d$, where the electric field in the x and the y direction has to be zero. This leads to an additional index l counting the number of variations in the standing wave pattern in the z direction of the TE_{mnl} or the TM_{mnl} mode as the indices m and n do for the x and y direction, respectively. The resonant frequency of the TE_{mnl} or the TE_{mnl} mode is determined by

$$f_{mnl} = \frac{1}{2\pi\sqrt{\mu\epsilon}}\sqrt{\left(\frac{m\pi}{a}\right)^2 + \left(\frac{n\pi}{b}\right)^2 + \left(\frac{l\pi}{d}\right)^2}. \tag{25}$$

The dominant resonant mode is the TE_{101} mode as it has the lowest resonant frequency. In Ref. [8] the internal quality factor of the cavity considering lossy conducting walls for the TE_{10l} modes is found to be

$$Q_c = \frac{(kad)^3\, b\eta}{2\pi^2 R_s}\,\frac{1}{2l^2a^3b + 2bd^3 + l^2a^3d + ad^3}. \tag{26}$$

The wall surface resistance R_s (see equation (8) and η (see equation (9)) are given in section 2.1.

3 Simulations

3.1 Introduction

The overall setup consists of two 3D microwave cavities that are coupled via a rectangular waveguide. The coupling from the cavity into the waveguide is obtained by a circular aperture, which acts as a shout inductance. Coaxial cables are used for the coupling from outside into each of the cavities. The purpose of the simulations is to characterize different aspects of this system. First, we focus on the study of rectangular waveguides, where the impact of various defects on the transmission is analyzed. Second, the coupling into the cavity via coaxial cables is investigated. In this case the resonance frequency and the quality factor for different configurations is calculated numerically. Third, the coupling from the cavity into the waveguide is simulated for different values of the radius of the aperture and the thickness of the separating wall.

3.1.1 COMSOL

All the simulations were done using the RF (Radio Frequency) module of the finite element solver COMSOL (version 4.3b), with which we can simulate electromagnetic wave propagation in waveguides and cavities. Furthermore, COMSOL computes the electromagnetic field distributions, the Q-factors and the S-parameters [4]. The chosen physics in COMSOL was 'Radio Frequency: Electromagnetic Waves, Frequency Domain (emw)' and the chosen study type was either 'Eigenfrequency' or 'Frequency domain'.
First, the models are designed in 3D. Next, different materials were allocated to the domains and surfaces. It is convenient to define collections of domains and surfaces of the same material using the 'create selection' symbol. In this way the material properties and boundary conditions can be allocated faster. In the next step the ports are defined. As input ports are used either 'rectangular' (waveguides) or 'coaxial' (coaxial cable) ports. In both cases the wave excitation at this port is on and the input power is 1 W. The lowest mode is selected. At the output port the wave excitation is turned off. The model is completed by defining a mesh for the finite element solver used to calculate the electromagnetic wave propagation. The quality of the outcome depends on the mesh parameters size. The meshes were usually customized for the given model. A maximum element size of one sixth of the investigated wavelength seems to be a good starting point.
After finalizing the model, a study can be performed. The study 'Frequency Domain' can be used to find the electric field distribution and the

S-parameters for a frequency or a range of frequencies. Moreover, it is possible to vary one or more parameters using a parametric sweep. All the system parameter values can be stored under 'Global Definitions→Parameters'. In this way the geometric model adjusts itself automatically when a parameter is changed or varied using parametric sweep. The study 'Eigenfrequency' can be used to calculate eigenfrequencies and Q-factors. The search for eigenfrequencies should be done around a desired frequency as can be chosen in the study settings[2].
After the simulation the outcome of the study is accessible under 'Results'. The electric field distribution is generated automatically. Using '1D Plot Group' plots of the S-parameters, the Q-factors or frequencies for different variables of the parametric sweep can be generated. Using 'Global Evaluation' these values can also be displayed in a table and exported.

3.1.2 Parameters

The simulations are done for the rectangular waveguides WR90 and WR137 (see dimensions in Table 1) made out of a metal with an electrical conductivity $\sigma = 10^{10}$ S/m and vacuum inside. For the coaxial cables the same conductivity $\sigma = 10^{10}$ S/m is used for the outer conductor (aluminum). For the inner conductor (silver plated copper) an electrical conductivity $\sigma = 10^{8}$ S/m is assumed. The coaxial cable contains PTFE as a dielectric with a relative permittivity $\epsilon = 2.1$ and zero electrical conductivity. For the waveguides the calculations are done at a frequency of 7.9 GHz for the WR137 waveguide and 10 GHz for the WR90 waveguide. The cavities are chosen to have the same dimensions a and b as the waveguide coupled to them. The length d of the cavity is selected such that the eigenfrequency of the cavity is around 7.9 GHz or 10 GHz, respectively. Using equation (25) this results in $d = 22.64$ mm for WR137 and $d = 19.88$ mm for WR90.

[2]When starting the study, usually an error is output after a short study time and under 'Solver Configurations→Solver 1→Eigenvalue Solver 1→Values of Linearization Point' a transform point can be chosen. Setting that value to the foreknown bare eigenfrequency allows the study to converge.

3.2 The influence of errors in the waveguide

In this section we investigate the influence of small errors in the construction of the waveguide on the transmission properties. Since the total distance between the two cavities has to be more than 10 m, the waveguide will probably consist of more then one waveguide piece, which may lead to imperfections at the different interfaces. The investigated errors include a weld seam which can be curved inward ('Inner seam') or outward ('Outer seam'), the waveguide being bent in the propagation direction ('Bend') and two waveguides being rotated at their connection point ('Rotation'). Furthermore, the effect of one and many pyramid formed defects inside the waveguide is tested. For all simulations one input and one output port at the ends of the waveguide are chosen and the S-parameter S21 is obtained. For a comparison of the transmission loss due to defects, the S21 parameter of a waveguide of 20 cm without any errors is simulated first. The transmission is frequency dependent: the higher the frequency, the higher the S21 parameter (see Figure 5). For the WR137 waveguide a value of $-3.90 \cdot 10^{-3}$ dB/m was obtained for the S21 parameter at 7.9 GHz. For the WR90 waveguide the S21 parameter has a value of $-8.25 \cdot 10^{-3}$ dB/m at 10 GHz. The same values are obtained for the attenuation coefficients using equation 7. The S21 parameter scales linearly with the length of the waveguide.

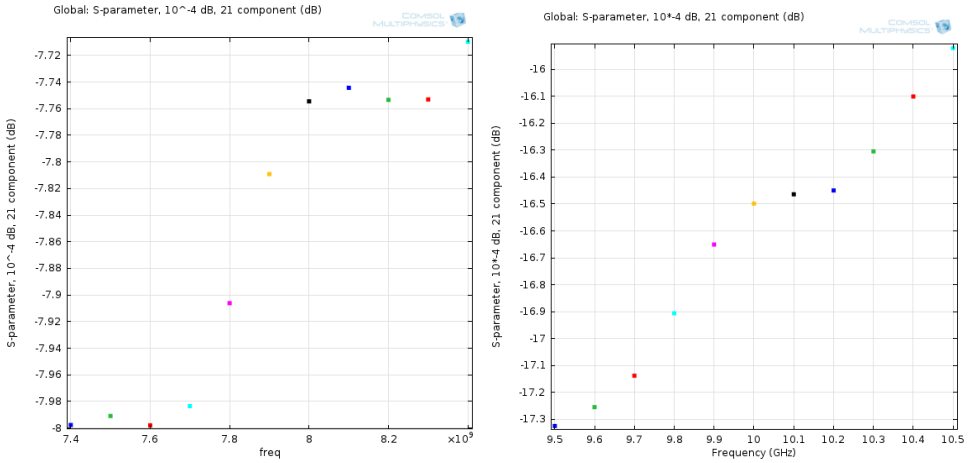

(a) *WR137 waveguide* (b) *WR90 waveguide*

Figure 5: *S21 parameter in* 10^{-4} *dB for different frequencies for 20 cm long waveguides without any defects.*

3.2.1 Inner seam

At the connection to a flange or if two waveguides are welded together, usually a seam is obtained on the inside of the waveguide. In the simulation this is implemented by intersecting four cylinders of radius r with the cuboid representing the waveguide (compare with Figure 6a). The seam effects the electric field inside the waveguide as can be seen in Figure 6b. The electric field is enhanced at the upper and lower part of the seam, whereas it does not change on the sides of the waveguide since the TE10 mode is zero. Part of the wave is reflected back by the cylindrical defect and a standing wave is obtained.

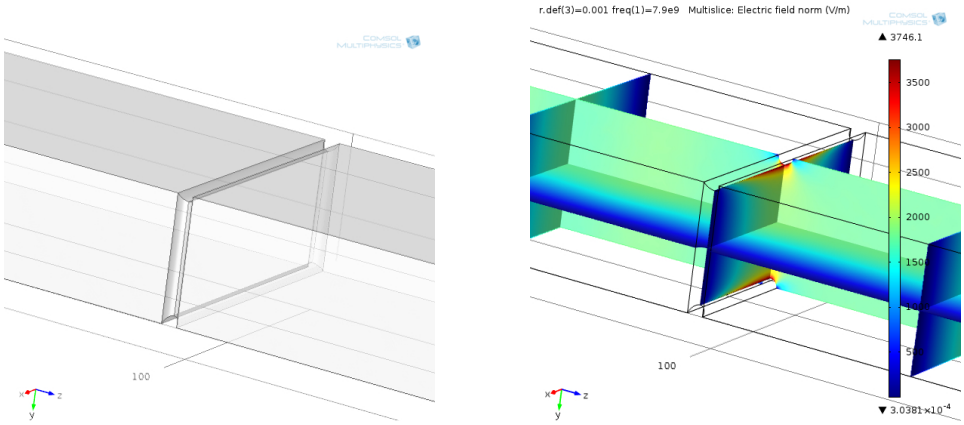

(a) *Model inner seam consisting of 4 cylinders.*

(b) *Norm of the electric field for the inner seam model of the WR137 waveguide.*

Figure 6: *Inner seam model.*

As a result, a reduced S21 parameter is found. The loss is higher for a larger radius. The change in the S21 parameter when varying the radius can be seen in Figure 7 for the WR137 waveguide at 7.9 GHz. Qualitatively, the simulation shows a similar shape for the WR90 waveguide. The S21 parameters obtained from the simulations for 5 different radii are shown in Table 2. A radius of 0.1 mm has no effect on the S21 parameter, while a radius of 0.5 mm leads to a decrease of the S21 parameter by 27% for the WR90 waveguide and 38% for the WR137 waveguide. For a 1 mm inner seam, the loss is about 4 to 7 times as high as in the defect free model. A radius of 2 mm on both sides corresponds to a fraction of 40% of the shorter side b of the WR90 waveguide being distorted. Therefore, inner seams above

0.5 mm radius should be avoided.

Radius of defect	S21 for WR137 in 10^{-4} dB	S21 for WR90 in 10^{-4} dB
no defect	-7.81	-16.5
0.1 mm	-7.80	-16.5
0.5 mm	-10.8	-21.0
1.0 mm	-48.9	-74.8
1.5 mm	-203	-269
2.0 mm	-595	-679

Table 2: *S21 parameters for different radii of inner seam defects*

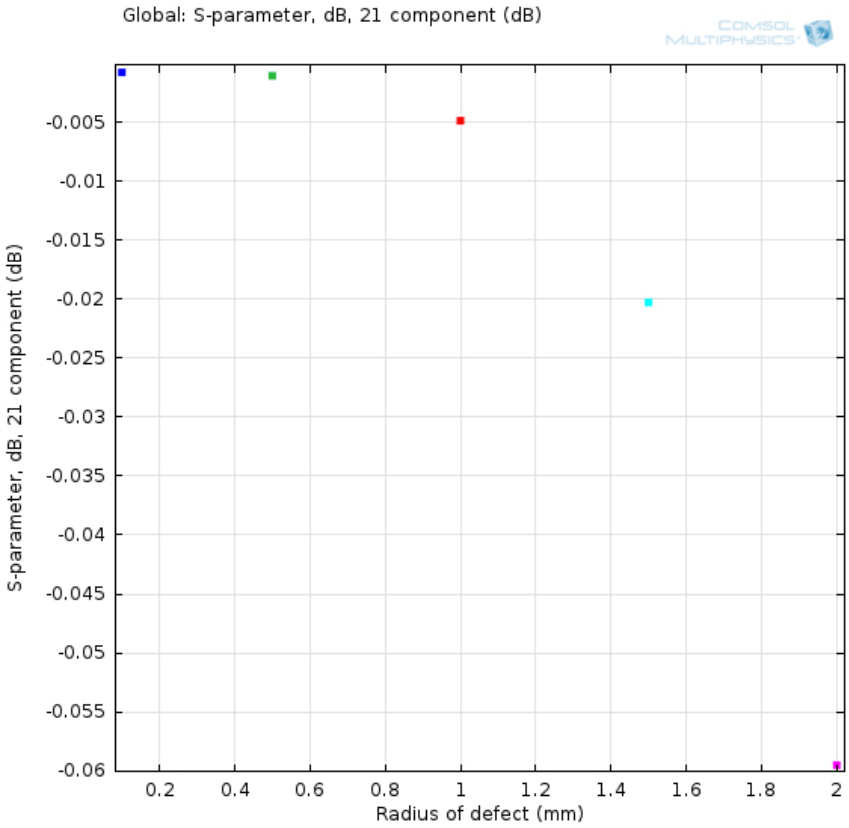

Figure 7: *S21 parameter in dB for different radii at 7.9 GHz for the 20 cm long WR137 waveguide with an inner seam defect in the middle.*

3.2.2 Outer seam

The seam does not necessarily have to be bent inward but could also be bent outward. For this model the same cylindrical approach is used. The same effects as in the inner seam model are found; reflections lead to a standing wave and the electric field is enhanced only at the edge (Figure 8). Inside the half-cylindrical bent the electric field is zero even at the maximum of the electric field of the TE_{10} mode. In this model the radius of the cylinders is also varied and the simulation of the S21 parameters for different radii leads to a qualitatively similar shape as for the inner seam. For comparison with the inner seam, all values are summarized in Table 3. The outer seam reduces the transmission less than the inner seam does, which can be explained by the electric field not penetrating into the new cylindrical cavity.

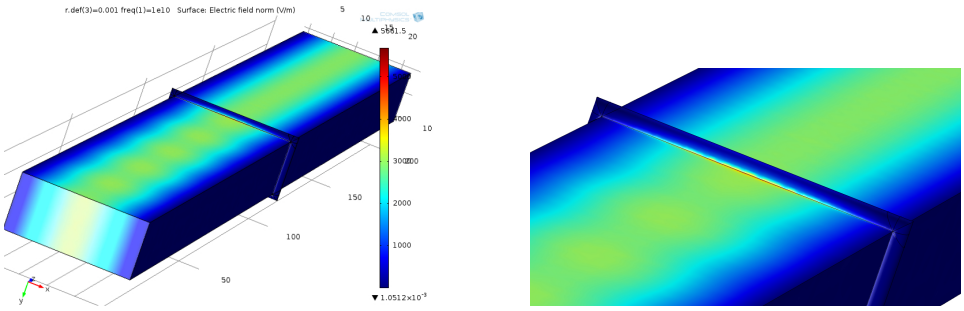

(a) *Standing wave between input port and defect.*

(b) *Norm of the electric field at the defect.*

Figure 8: *Norm of the electric field in the outer seam model.*

	S21 in 10^{-4} dB			
	WR137		WR90	
Radius of defect	inner seam	outer seam	inner seam	outer seam
no defect	-7.81	-7.81	-16.5	-16.5
0.1 mm	-7.80	-7.80	-16.5	-16.5
0.5 mm	-10.8	-8.35	-21.0	-18.3
1.0 mm	-48.9	-19.5	-74.8	-49.1
1.5 mm	-203	-70.8	-269	-187
2.0 mm	-595	-211	-679	-561

Table 3: *S21 parameters for different radii of seam defects.*

3.2.3 Bend

A waveguide might be bent because two waveguides are not aligned properly. In this model the 20 cm waveguide is bent in the middle by different bending angles, which leads to a change in the electric field. Figure 9 shows that the electric field is higher in the inner bend compared to the outer bend.

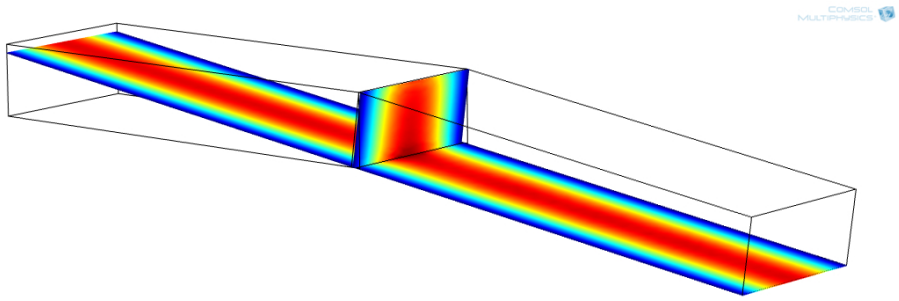

Figure 9: *Norm of the electric field for a WR137 waveguide bent by 10°.*

The graph of the S21 parameter as a function of bending angle (see Figure 10) has a similar shape as the one for the inner or outer seam. Some values for the S21 parameters of the WR137 and WR90 waveguides are listed in Table 4. For small bending angles up to 5° the change in the S21 parameter is less than 1%. If higher precision ought to be obtained, the mesh size has to be made smaller in order to receive sensible values. A bending angle of 10° leads to 20% more loss in the WR137 waveguide and only 4% more loss in the WR90 waveguide. The WR90 waveguide is less sensible to bending. At an angle of 20° the WR90 waveguide has less loss than the WR137 waveguide. For larger bending angles than 10° the S21 parameter drops drastically and reaches 4.38 dB at 90° for the WR137 waveguide and 1.1 dB for the WR90 waveguide. Part of the wave is reflected at the bend and a standing wave is obtained, which reduces the transmission. For the 10 m waveguide project, bending should not be a problem as a bending angle of 1°, which does not affect the transmission, would correspond to a change in height of 17 cm.

Bending angle	S21 for WR137 in 10^{-4} dB	S21 for WR90 in 10^{-4} dB
no defect	-7.81	-16.5
2°	-7.82	-16.5
4°	-7.86	-16.5
6°	-8.00	-16.5
8°	-8.34	-16.7
10°	-9.34	-17.1
20°	-35.4	-26.9
30°	-159	-72.2

Table 4: *S21 parameters for different bending angles for the 20 cm long WR137 and WR90 waveguide.*

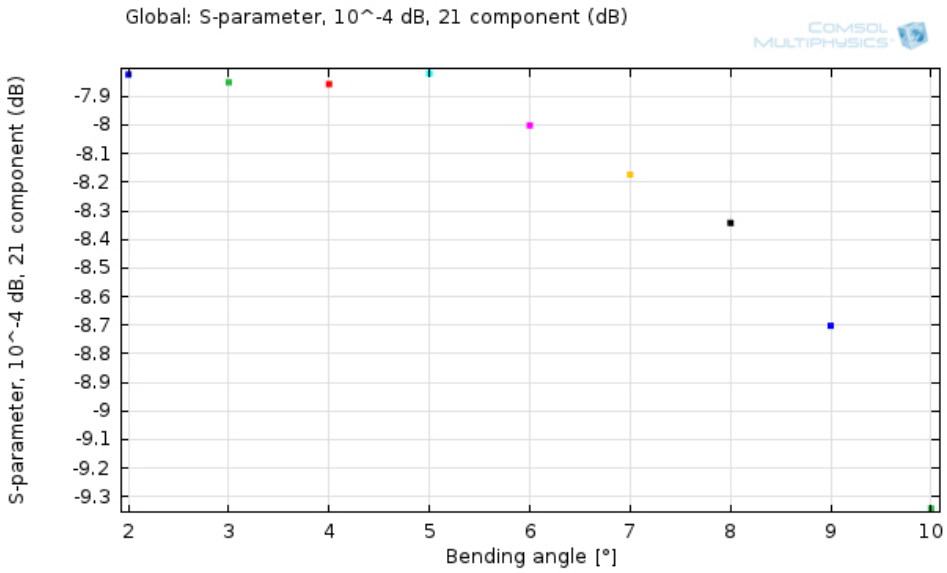

Figure 10: *S21 parameters for different bending angles of the WR137 waveguide.*

3.2.4 Rotation

At the intersection points, where two pieces of a waveguide are screwed together, a rotation can occur along the long axis. In this model flanges have to be included to simulate the defects due to the rotation. At the intersection a sharp kink appears and the flange protrudes (see Figure 11). Due to the flanges the waveguide is only open for rotation angles of around 10°. In the simulations 'impedance boundary condition' can not be assigned to the inside surfaces of the flanges because they have a metal bulk piece behind them. So the option 'perfect electric conductor' is chosen for that part. In a perfect electric conductor the electric field does not penetrate the surface while the option 'impedance boundary condition' allows for an exponential decay of the electric field inside the material, which leads to loss. In this case the reference system corresponds to a rotation angle of 0° because it contains a loss-less perfect conductor surface in contrast to the other cases.

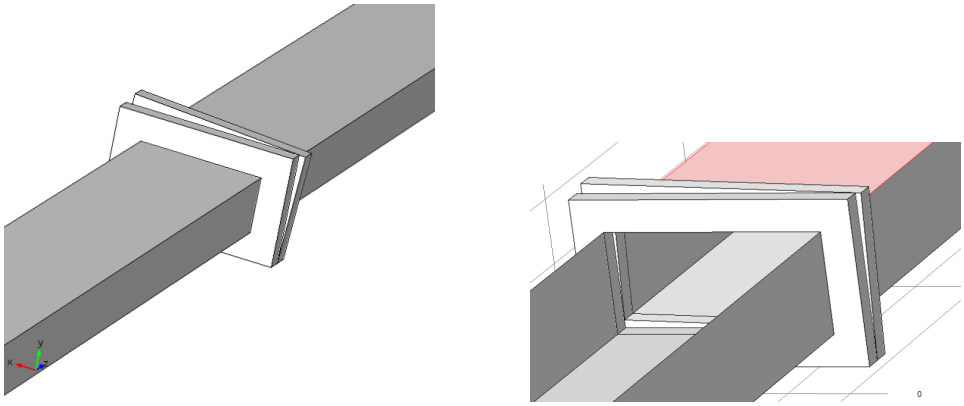

(a) *2 WR137 waveguides rotate by 2° with respect to each other.*

(b) *Inside view: the white surface of the flange can be seen.*

Figure 11: *Rotated waveguide model.*

The values for the S21 parameters in the rotation model are displayed in Table 5. The dependance of S21 on the rotation angle shows a similar curve as for the bending angle. The dependance of the rotation angle is however stronger. Therefore the waveguides should be properly aligned in this direction. Again the WR90 waveguide is more robust to rotation defects, but has a higher resistive loss without defects.

Rotation angle	S21 for WR137 in 10^{-4} dB	S21 for WR90 in 10^{-4} dB
0°	-7.57	-16.0
1°	-7.76	-16.1
2°	-9.05	-16.5
3°	-13.4	-17.9
4°	-23.7	-21.2
5°	-43.8	-27.6
6°	-78.6	-38.1
7°	-134	-54.8
8°	-217	-79.4
9°	-336	-113
10°	-500	-160

Table 5: *S21 parameters for different rotation angles for the 20 cm long WR137 and WR90 waveguide.*

3.2.5 Pyramid defect

In order to simulate a point defect inside the waveguide, an object with the shape of a pyramid as shown in Figure 12(a) was chosen. Such defects can for example arise from production errors and dirt deposition. The shape of the defect should not be symmetric in order to avoid special behavior like standing waves due to the symmetry of the system. Therefore, a pyramid seems to be an appropriate choice which COMSOL offers. The pyramid concentrates the electric field at its peak (compare Figure 12(b)).

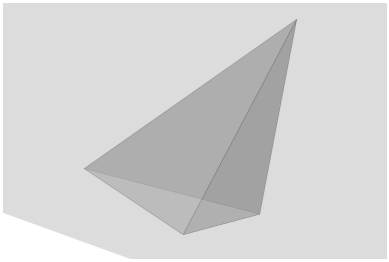

(a) *The pyramid used in the pyramid models.*

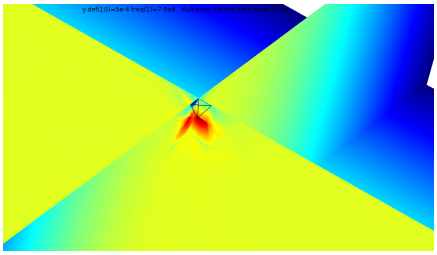

(b) *The modified electric field around the pyramid defect.*

Figure 12: *The pyramid model.*

In this simulation the height of the pyramid is varied and the S21 parameter is investigated. The result is displayed in Figure 13 for the WR137 waveg-

uide. The curve shows a similar shape for both waveguides. For heights up to 0.8 mm no significant effect can be observed in Table 6.

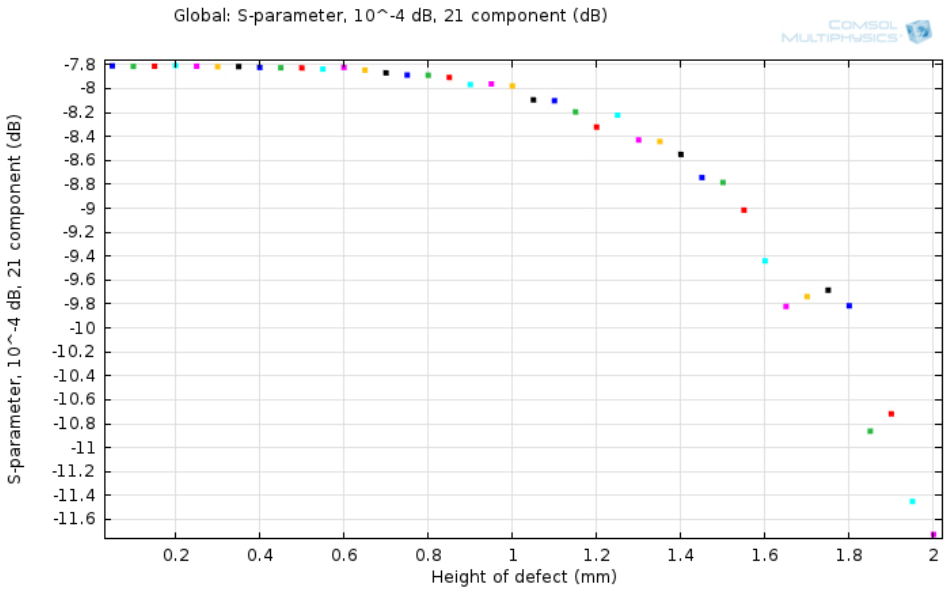

Figure 13: *One pyramid: S21 parameter in* 10^{-4} *dB for different heights of the pyramid defect at 7.9 GHz for the 20 cm long WR137 waveguide.*

3.2.6 Many pyramid defects

In the real waveguide the whole surface is rough. This is simulated by using a large amount of pyramid defects. Due to limited computational resources, the amount of pyramids is limited to 45. Using the 'copy' option in COMSOL, the pyramid is duplicated and displaced, which leads to a grid of pyramids as it is shown in Figure 14. The dimensions of the pyramids can be varied up to 1 mm because the pyramids intersect. For larger dimensions this leads to boundaries with wrongly defined boundary conditions. Table 6 indicates that the difference between one or 45 pyramid defects is below 7% for the WR137 waveguide and below 20% for the WR90 waveguide for the simulated dimensions. The focus should therefore lay on minimizing the height of the defects instead of the number of point defects.

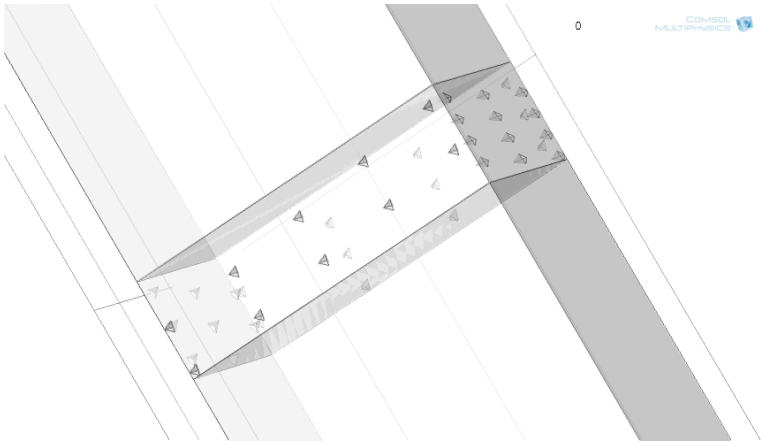

Figure 14: *The surface with 45 pyramid defects.*

	S21 in 10^{-4} dB			
	WR137		WR90	
Height of pyramid	1 pyramid	45 pyramids	1 pyramid	45 pyramids
no defect	-7.81	-7.81	-16.5	-16.5
0.1 mm	-7.81	-7.81	-16.5	-16.5
0.2 mm	-7.81	-7.81	-16.5	-16.5
0.4 mm	-7.82	-7.83	-16.5	-16.6
0.6 mm	-7.82	-7.91	-16.6	-16.9
0.8 mm	-7.89	-8.18	-16.9	-18.3
1.0 mm	-7.97	-8.56	-17.4	-20.9

Table 6: *S21 parameters for different heights of pyramid defects.*

3.2.7 Conclusion

The S21 parameter shows the same dependance on the size of the imperfection for all the different kind of defects. The main difference is the magnitude of the effect. It is obvious that defects should be as small as reasonably achievable. The simulation results can be used to decide if a certain type of imperfection should be made smaller. The results also give suggestions on how the waveguides can be constructed. Some defects can be minimized or avoided easier than others. Therefore one should focus on those that can be minimized easily or lead to a relatively large improvement in the transmission.

3.3 Coupling into the cavity

In this section the coupling between a coaxial cable and a 3D cavity is investigated. For the coaxial cable the parameters of the UT-085C-Al-TP-LL cable is used. This cable has a outer conductor with radius $R = 1.09855$ mm made out of aluminum and an inner conductor with radius $r = 0.287$ mm made out of silver plated copper [6]. Between the two conductors PTFE is used as a dielectric filling. Inside the cavity vacuum is assumed. The electrical conductivities and the relative permittivity for the materials are stated in section 3.1.2. For the cavity the dimensions a and b of the WR137 waveguide are used. The eigenfrequency of the cavity is chosen to be 7.9 GHz by adapting the length d. In the model two coaxial cables are attached to the top of the waveguide. One will act as the input port and the other as the output port. Figure 15a gives an overview of the model. In the simulations two main questions are examined:

- How does the position of the coaxial cable on the surface of the cavity influence the loaded, the internal and the external quality factor of the system? How is the coupling affected?
- How does the length of the inner conductor and dielectric extending into the cavity influence the coupling?

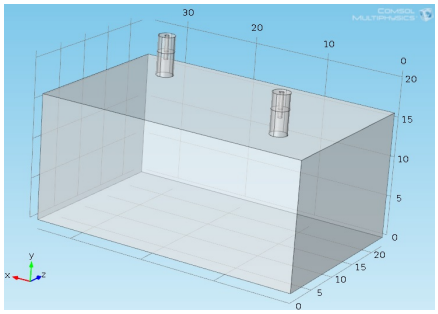

(a) *The model - an overview.*

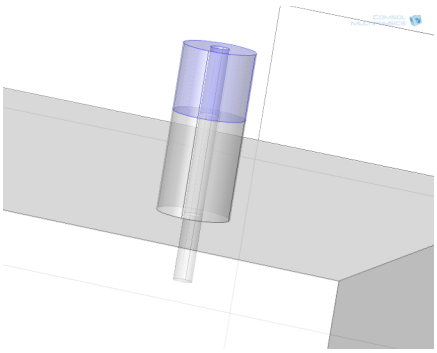

(b) *The coaxial cable with the dielectric in blue 3 mm above the surface of the cavity. The cylinder with the small radius is the inner conductor, the other the outer conductor.*

Figure 15: *Model of the two coaxial cables coupled to the cavity.*

3.3.1 Influence of the position of the coaxial cable

The question concerning the influence of the position of the coaxial cable will be answered first. Using the model described above, three values will be varied:

- The position in x-direction: coaxX
- The position in z-direction: coaxZ
- The length of the inner conductor protruding from the dielectric: coaxin

The coordinates are chosen such that the cavity has width a in x-direction, height b in y-direction and length d in z-direction. Since the cavity surface is point symmetric to the center, the positions of the input coaxial cables are only varied in one forth of the surface as it is depicted in the schematic of Figure 16. The cables are placed periodically with a distance of 4 mm in x-direction and 3 mm in y-direction. The starting position is chosen so that the last cable in each row or column is positioned in the middle. In each simulation one cable is used as the input and the other as the output cable. The two cables are placed point symmetrically with respect to the center of the surface. Therefore the middle coaxial cable is left away.

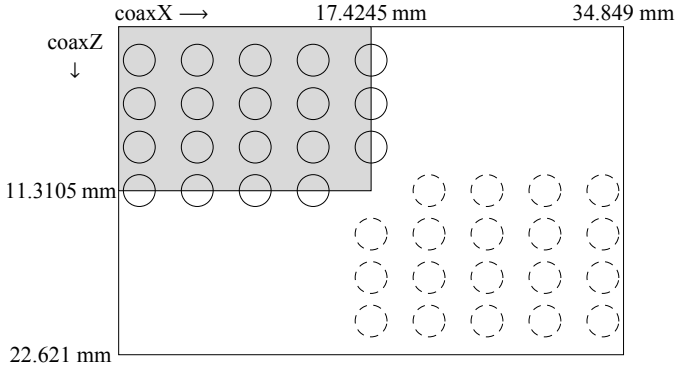

Figure 16: *The big rectangle represents the top surface of the cavity. The black circles are the positions of the input coaxial cable, the dashed circles belong to the output cables placed symmetrically to the center. The position of the input cables is labeled with coaxX along the horizontal axis and with coaxZ along the vertical axis.*

For each of the 19 positions the length of the inner conductor sticking out of the dielectric is varied from 1 mm to 4 mm. The outer conductor is attached to the cavity and the dielectric is cut off 3 mm above the cavity (compare with Figure 15b). This means that for coaxin = 3 mm the inner conductor is at the same height as the surface of the cavity, for coaxin = 4 mm it emerges 1 mm into the cavity. In a first set of simulations the resonant frequency f_0 and the loaded quality factor Q_L of the system is computed. This data is then used to calculate the appropriate frequency spectrum over which the S_{21} parameter should be computed. The bandwidth δf of the Lorentzian function can be assessed using equation (18). The calculated bandwidth is doubled in order to cover a nice range of the Lorentzian function and then divided into 20 equally spaced frequency points at each side of the resonant frequency. The simulation is run to calculate the S_{21} parameter for each of the 41 frequencies at each position of the coaxial cable. The data sets are exported and analysed with Mathematica, where the fitting routine for the Lorentzian function is done. An characteristic example can be seen in Figure 17.

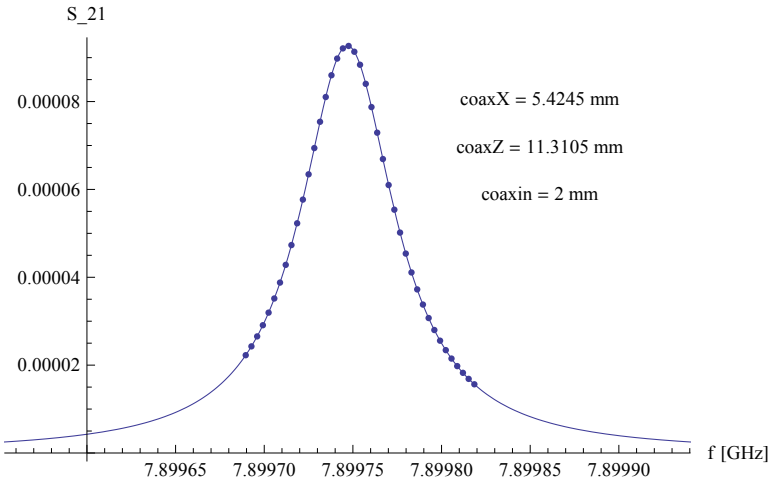

Figure 17: *A Lorentzian fit for the S_{21} parameter as a function of frequency. The input coaxial cable is positioned at the place indicated on the figure.*

The loaded quality factor extracted from the Lorentzian fit is in agreement with the one which COMSOL computed. Using equation (22) and (23), the external and internal quality factor is calculated. The internal quality factor is between 112'000 and 130'000 for all configurations. The external quality factor is highly dependent on the length the coaxial cable protruding from

the dielectric. For 1 and 2 mm the external quality factor is above 10^8 for coaxin = 1 mm and above 10^6 for coaxin = 2 mm. This means that the loaded quality factor is about as high as the internal quality factor. For a length of 3 or 4 mm, when the inner conductor of the coaxial cable reaches the surface of the cavity (coaxin = 3 mm) or extends into the cavity (coaxin = 4 mm), the coupling is strongly increased. The loaded quality factor Q_L depends also on the position of the coaxial cable on the surface of the cavity. This can be seen in Figure 18. Positions which are closer to the center lead to stronger coupling into the TE_{101} mode of the cavity. This can be explained by the mode structure.

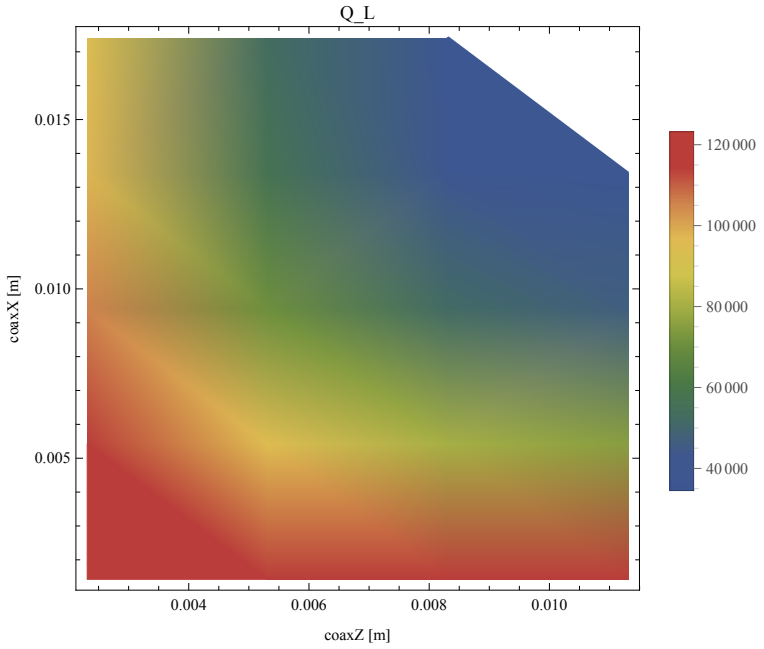

Figure 18: *The loaded quality factor for different positions of the coaxial cable in x-direction (coaxX) and in z-direction (coaxZ) with coaxin = 3 mm.*

Focusing on one fixed position in z-direction, the dependence of the quality factors on the x-position coaxX can be investigated in more detail. This is done in Figure 19. For x-positions of the coaxial cable on the side of the cavity, the external quality factor is larger than Q_{int}. Moving the cable towards the center leads to a decrease in the external quality factor (see Figure 20a) because the coupling into the TE_{101} mode of the cavity is stronger in the center.

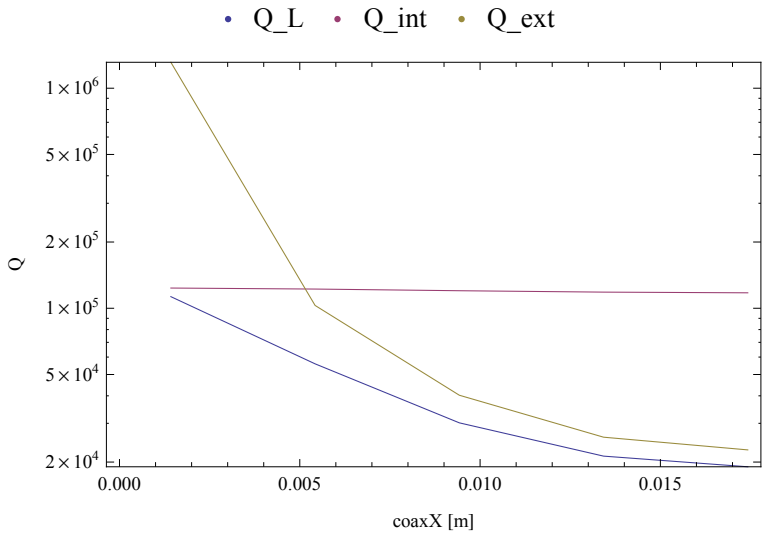

(a) *The z-direction was fixed at coaxZ = 2.3105 mm.*

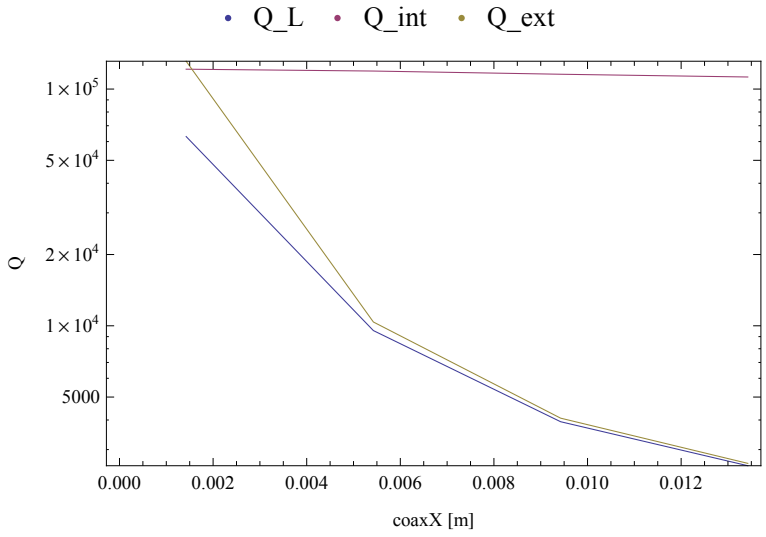

(b) *The z-direction was fixed at coaxZ = 11.3105 mm.*

Figure 19: *The loaded quality factor (blue), the internal quality factor (purple) and the external quality factor (green) for different positions of the coaxial cable in x-direction. The length of the inner conductor sticking out of the dielectric was 4 mm.*

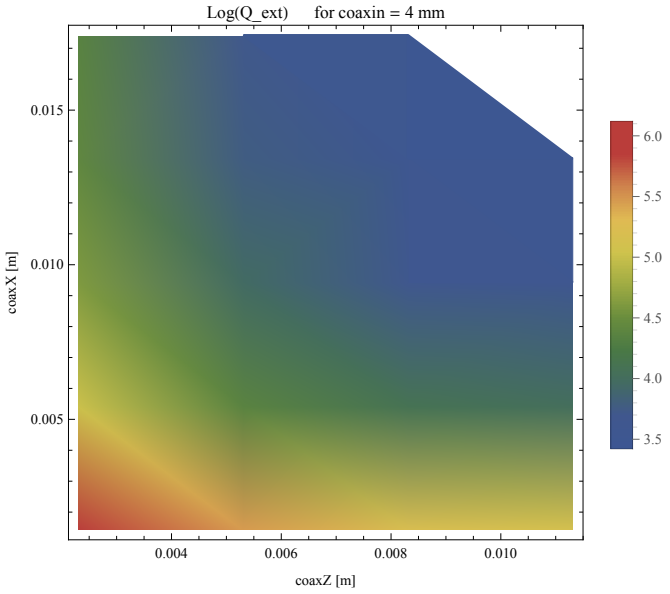

(a) *The logarithm of the external quality factor.*

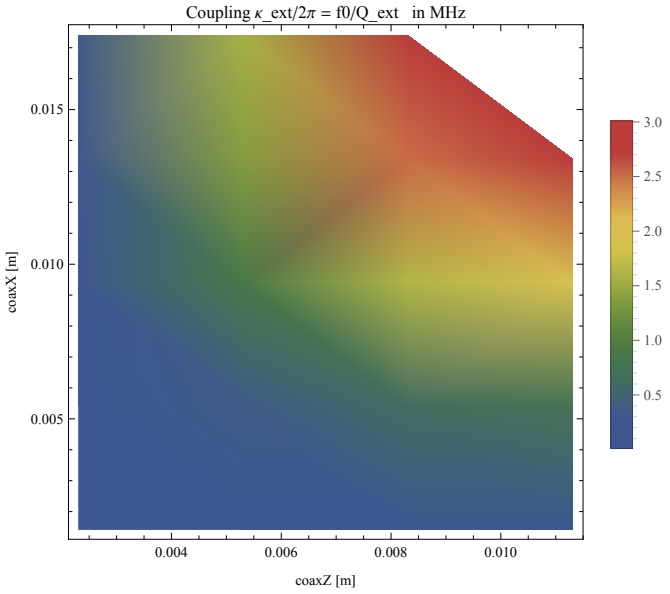

(b) *The external coupling $\kappa_{ext}/2\pi$ in MHz*

Figure 20: *The logarithm of the external quality factor and the external coupling coefficient in MHz for different positions (coaxX, coaxZ) of the coaxial cable and with coaxin = 4 mm.*

For positions closer to the center Q_{ext} reaches the internal quality factor Q_{int}, where critical coupling is achieved, and continues to decrease. Here the loaded quality factor is dominated by the external one and is at a minimum close to the center of the cavity surface. The coupling between the coaxial cables and the cavity can be characterized by the external coupling coefficent $\kappa_{ext}/2\pi$ given by equation (24) and plotted in Figure 20b.

3.3.2 Influence of the conductors and the dielectric

In the previous section we have seen that the external quality factor depends on the position of the coaxial cable and the length of the inner conductor. In order to investigate the effect of the length of the inner conductor and the position of the dielectric above the cavity, the position of the cable is fixed to one specific position (coaxX = 6.4245 mm, coaxZ = 6.13105 mm). In the first layout, the length of the inner conductor sticking out of the dielectric is varied from coaxin = 0 mm (cut off at the same place as the dielectric) to coaxin = 5 mm (extending 2 mm into the cavity). In the second layout, coaxin is fixed to 2 mm while the whole dielectric and inner conductor combination is varied from 3 mm above the cavity down to the surface of the cavity. Figure 21 illustrates the different layouts. A third layout where the inner conductor is cut off right at the dielectric (coaxin = 0 mm) is also calculated and the same characteristics can be seen.

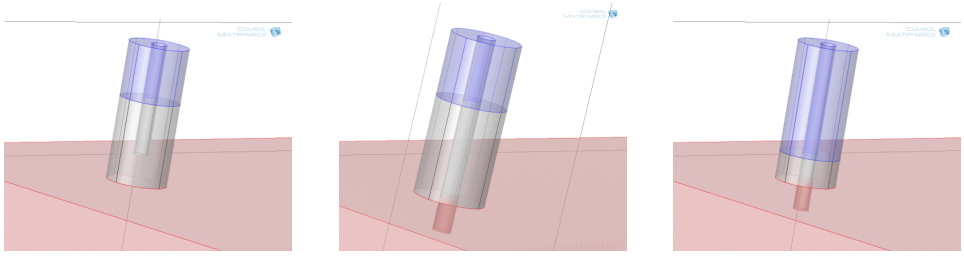

(a) *Layout 1 and 2. With coaxin = 2 mm and the dielectric 3 mm above the cavity.*

(b) *Layout 1. With coaxin = 4 mm and the dielectric 3 mm above the cavity.*

(c) *Layout 2. With coaxin = 2 mm and the dielectric 1 mm above the cavity.*

Figure 21: *The different layouts to analyse the influence of the conductors and the dielectric.*

Impact of the length of the inner conductor (Layout 1)
As in the previous simulation, the loaded quality factor and the resonant frequency are computed for different lengths of the inner conductor. These two values are then used to choose an appropriate frequency range for the frequency sweep. The different Lorentzian functions can be seen in Figure 22. The resonant frequency does not strongly depend on the inner conductor lengths between coaxin = 0 mm to coaxin = 3 mm and is 7.8997 GHz. If the inner conductor extends into the cavity, the resonant frequency is lowered - for example by 7.2 MHz for coaxin = 5 mm.

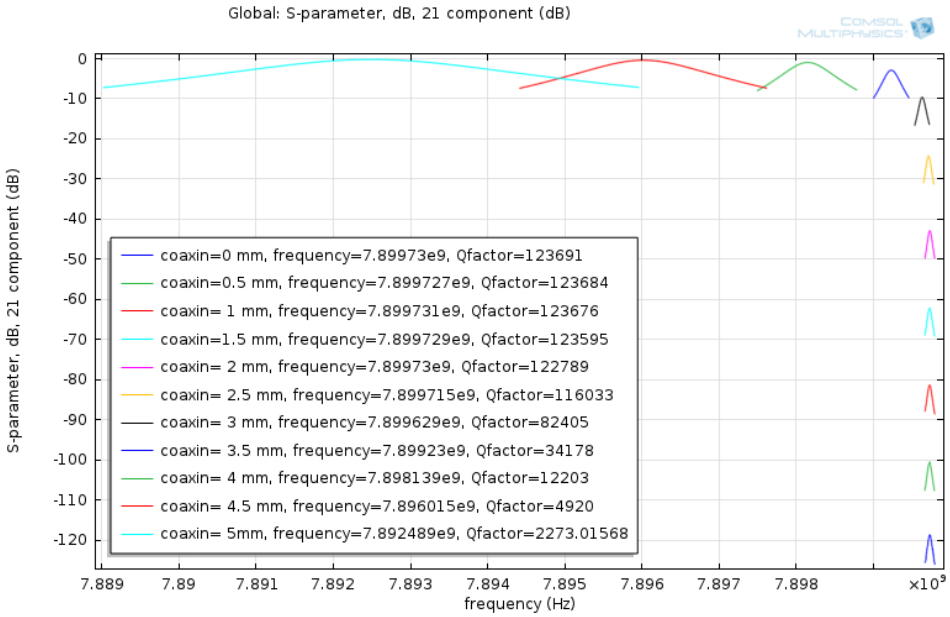

Figure 22: *The S21 parameter as a function of frequency around the resonance frequency for different length of the inner conductor sticking out of the dielectric (coaxin).*

From the Lorentzian fit, the internal and the external quality factors are obtained and displayed logarithmically in Figure 23. The internal quality factor varies from 109'000 to 125'000 as can be seen in Table 7. The external quality factor decreases exponentially with the length of the inner conductor protruding from the dielectric. At the chosen position of the coaxial cable on top of the cavity, the resonator is under-coupled if the inner conductor does not extend into the cavity.

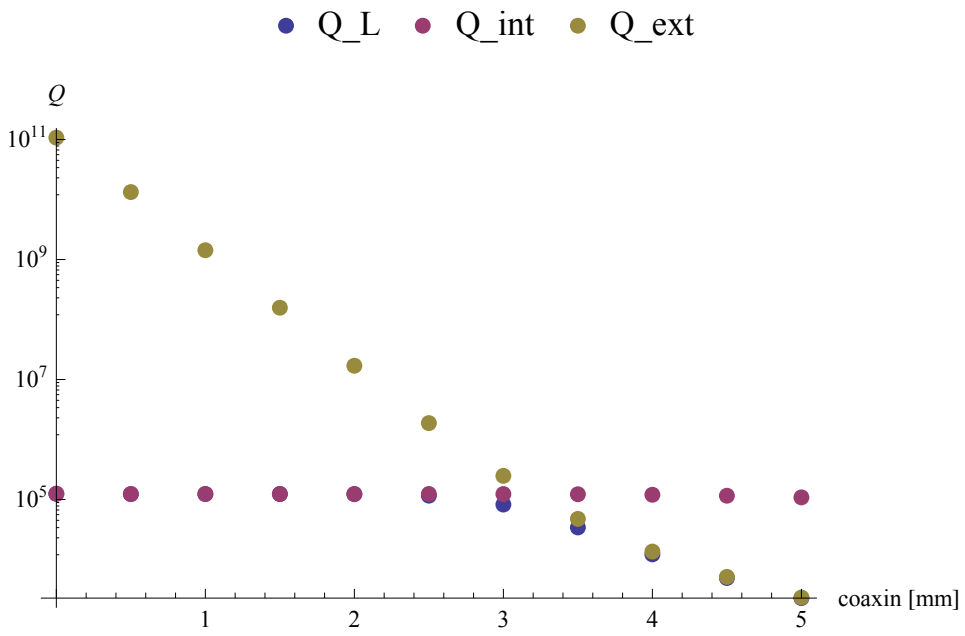

Figure 23: *The internal, external and loaded quality factors for different lengths of the inner conductor sticking out of the dielectric.*

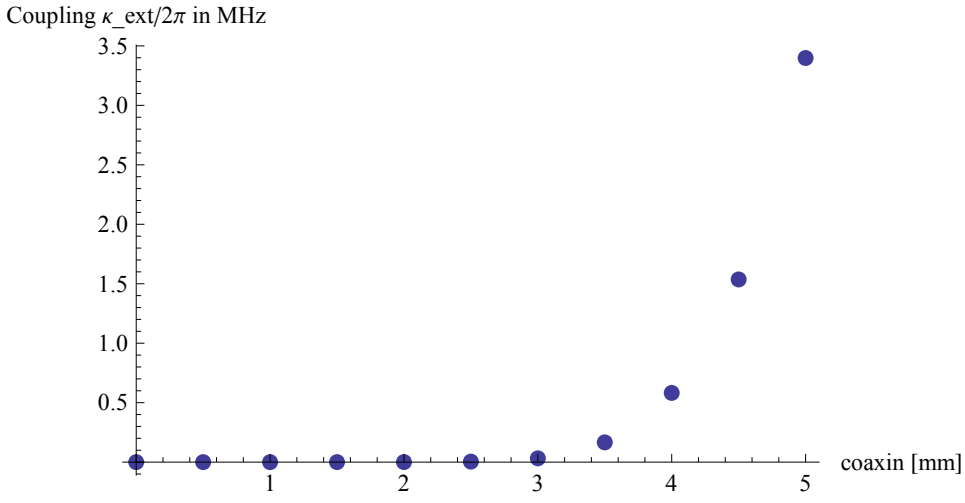

Figure 24: *The external coupling coefficient in MHz for different lengths of the inner conductor sticking out of the dielectric.*

The coupling between the coaxial cables and the cavity is described by the external coupling coefficent $\kappa_{ext}/2\pi$, which is plotted in Figure 24. The external coupling coefficient varies over 8 orders of magnitude from 0.07 Hz (coaxin = 0 mm) to 3.40 MHz (coaxin = 5 mm) as summarized in Table 7. If the inner conductor extends into the cavity, couplings in the MHz regime can be obtained. In conclusion, the external coupling can be chosen by varying the length of the inner conductor.

coaxin	$\kappa_{ext}/2\pi$	Q_{int}
0 mm	0.07 Hz	125'000
1 mm	5.53 Hz	123'000
2 mm	465 Hz	124'000
3 mm	31.8 kHz	123'000
4 mm	582 kHz	120'000
5 mm	3.40 MHz	109'000

Table 7: *The external coupling coefficient and the internal quality factor for different lengths of the inner conductor sticking out of the dielectric.*

Impact of the position of the dielectric (Layout 2)
The same analysis is done for layout 2, where the height of the dielectric above the cavity is changed. The length of the inner conductor protruding from the dielectric is fixed to 2 mm. Figure 25 shows that the coupling is larger for dielectric and inner conductor compositions that are close to the surface of the cavity. The values for the external coupling coefficient are displayed in Table 8 along with the internal quality factors. The internal quality factor is also influenced by the position of the dielectric, which is plotted in Figure 26. If the inner conductor does not extend into the cavity, Q_{int} has a constant value of 124'000. The internal quality factors are the same for both layout 1 and 2 for corresponding inner conductor end positions. This can be seen in the example of the inner conductor emerging 1 mm into the cavity: in layout 1 this corresponds to coaxin = 4 mm and in layout 2 to a dielectric of 1 mm height above the cavity. Both have an internal quality factor of 120'000. The external coupling is of the same order of magnitude for corresponding inner conductor end positions, but it is not the same for the two layouts if the inner conductor emerges into the cavity. In the example where the inner conductor emerges 1 mm into the cavity, the coupling is reduced in layout 2 with 490 kHz compared to layout 1 with 582 kHz. In layout 2 the dielectric covers more of the inner conductor and affects the coupling. In conclusion, the height of the dielectric above the cav-

ity does not influence the internal quality factor, but can have a screening effect reducing the coupling.

Height above cavity	0.2 mm	1 mm	2 mm	3 mm
$\kappa_{ext}/2\pi$	1.98 MHz	490 kHz	29.4 kHz	462 Hz
Q_{int}	113'000	120'000	123'000	124'000

Table 8: *The external coupling coefficient and the internal quality factor for different heights of the dielectric and inner conductor composition above the cavity.*

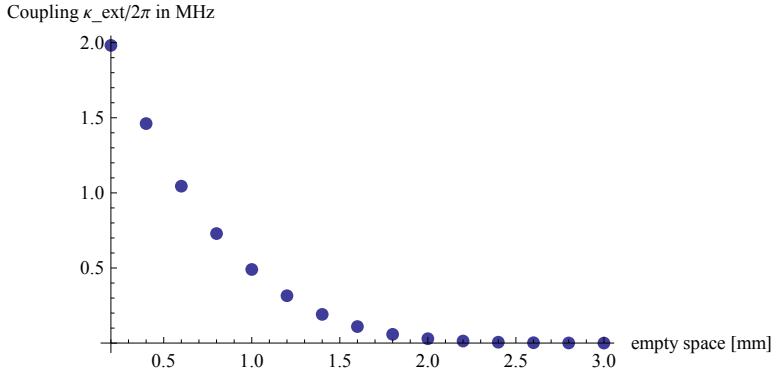

Figure 25: *The external coupling coefficient in MHz for different heights of the dielectric above the cavity.*

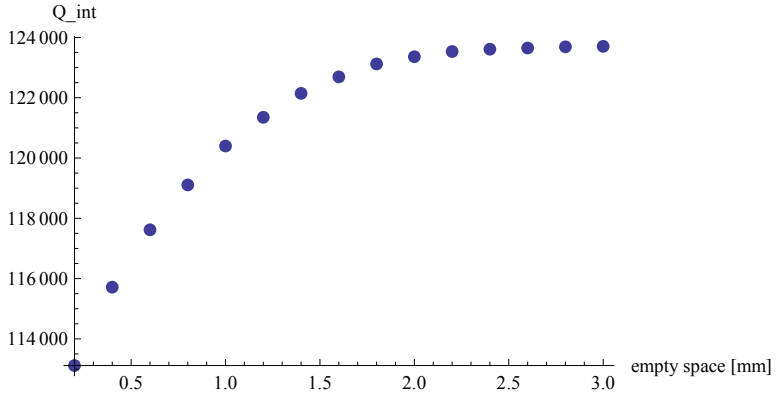

Figure 26: *The internal quality factor for different heights of the dielectric above the cavity.*

3.4 Coupling cavity and waveguide

The model of the cavity with the two coaxial cables is now extended by adding the waveguide. The coupling from the cavity to the waveguide can be conducted by a aperture in the cavity and the waveguide. This aperature may be circular or rectangular and can be positioned at various different places. An antenna can also be inserted. The size, shape and position of the aperture influences the internal quality factor of the cavity and the coupling to the waveguide. An analysis of the different options is therefore necessary. The cavity and the waveguide are separated by a wall which has a certain thickness in experiments and is not infinitesimally small as in literature [8]. In this project a circular aperture with radius 4 mm is chosen. In the model described below, the waveguide is coupled to the side of the cavity (see Figure 27) where the dimensions a and b of the cavity and the waveguide match. The coaxial cables are placed at the same positions as described in section 3.3.2. The dielectric ends 2 mm above the cavity surface and the inner conductor sticks 3 mm out of the dielectric.

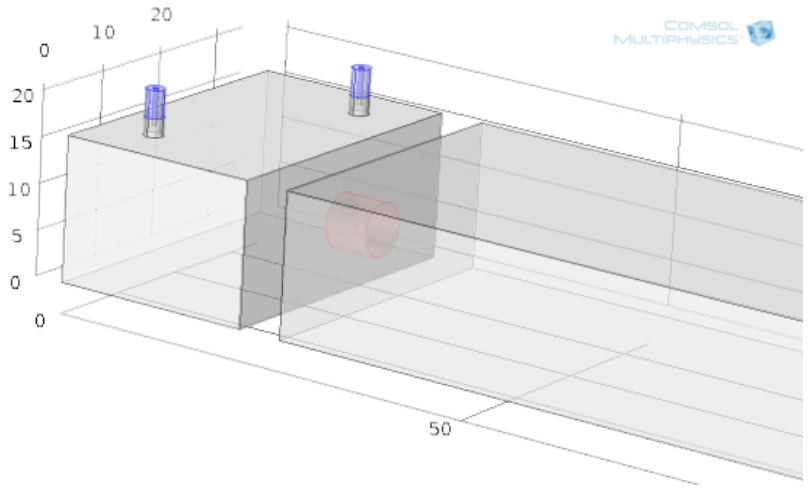

Figure 27: *The model of the cavity coupled to the waveguide.*

To investigate the coupling, three ports are defined:

- Input port 1 is the left coaxial cable.
- Output port 2 is the right coaxial cable.
- Output port 3 is at the end of the waveguide.

Same as in the other simulations, the resonant frequency and the loaded quality factor are obtained first and used to calculate the frequency range for the frequency sweep. Two different S-parameters are computed: the S21 parameter characterizing the transmission from one coaxial cable through the cavity to the other and the S31 parameter characterizing the transmission from the input coaxial cable into the cavity and through the waveguide. From the S21 and the S31 parameters two different sets of external quality factors are obtained (see Figure 28). The loaded quality factor is the same.

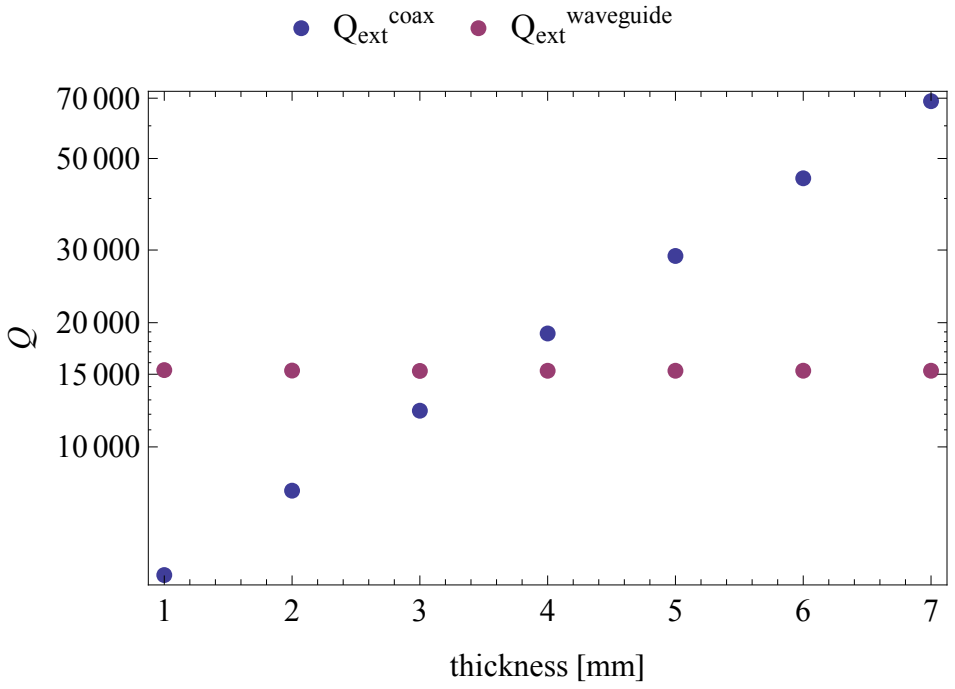

Figure 28: *The external quality factors for different wall thicknesses.* Q_{ext}^{coax} *is obtained from the S21 parameter and* $Q_{ext}^{waveguide}$ *from the S31 parameter. The radius of the hole is fixed to 4 mm.*

From the two external quality factors, the coupling between the coaxial cables and the coupling between the coaxial cable and the waveguide can be computed (see Figure 29). The coupling between the coaxial cables obtained from S21 does not depend on the thickness of the wall. For thicker walls the coupling from the coaxial cable into the waveguide is reduced. In this example the coupling into the waveguide is larger than the coupling into the coaxial cable for wall thicknesses below 3.5 mm. A thinner wall leads to a

larger coupling to the waveguide.

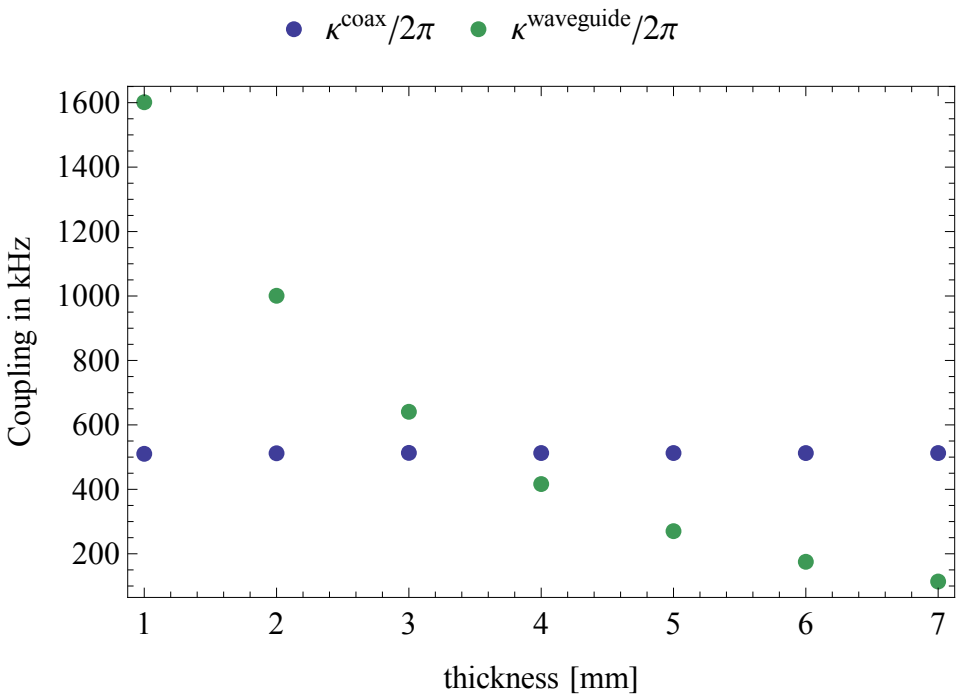

Figure 29: *The external coupling coefficients for different wall thicknesses.* $\kappa^{coax}/2\pi$ *describes the coupling between the coaxial cables in presence of a cavity and a waveguide (from S21).* $\kappa^{waveguide}/2\pi$ *describes the coupling into the cavity and through the waveguide (from S31).*

4 Conclusion

Rectangular waveguides show low transmission loss over long distances. Our simulations of different defects have shown that the transmission is not significantly affected by small defects. The obtained transmission tables for the different defects can be used to decide if the present defects should be minimized in experiments. They also give hints on how to construct a long waveguide.
In the second set of simulations, the coupling to the cavity through coaxial cables is understood. By varying the position of the coaxial cables on the surface of the cavity, the length of the inner conductor sticking out of the dielectric and the end position of the dielectric, the desired coupling can be engineered.
By adding the waveguide to the model of the cavity, the coupling to the waveguide can be simulated. One version of many was analysed in more detail. By choosing the thickness of the wall between the cavity and the waveguide as well as the radius of the hole, the coupling to the waveguide can be adjusted.

5 Outlook and Acknowledgements

The "SuperQuNet" project is still at the beginning and a lot of work has to be done until the loop-hole free Bell-Tests can be realized. Regarding the waveguide, the coupling from the cavity into the waveguide has to be investigated further. Many options are possible and only one is analyzed in this thesis. In order to optimized the system layout, the required coupling should be identified. At the moment parameters are varied to examine their general influence on the coupling strength without knowing which values to aim at. Also the whole system has not been simulated yet. Adding the second cavity and its two coaxial cables may lead to further changes in the transmission properties. Measurements of the attenuation of coaxial cables and waveguides are made at room and liquid helium temperature. Further measurements can be done concerning the coupling.

I would like to take this opportunity to thank Philipp Kurpiers for his guidance and assistance on the project. Many models and analysis were developped together. The discussions were fruitful and led to new insights. He also showed me how to measure S-parameters for coaxial cables and waveguides at room and liquid helium temperature. I have learned a lot and it

was a pleasure to work with Philipp Kurpier.
I would also like to thank Prof. Andreas Wallraff for giving me the option to work on this project. I enjoyed the nice atmosphere in the group.

References

[1] A. Aspect, et al., *Experimental Test of Bell's Inequalities Using Time-Varying Analyzers*, Phys. Rev. Lett. 49, 25, 1804 (1982).

[2] M. Ansmann, et al., *Violation of Bell's inequality in Josephson phase qubits*, Nature 461, 7263, 504 (2009).

[3] C. A. Balanis, *Circular Waveguides*, John Wiley & Sons, Inc. (2005).

[4] COMSOL, *RF Module*, http://www.comsol.com/rf-module (23.9.2013).

[5] M. Göppl, A. Fragner, M. Baur, R. Bianchetti, S. Filipp, J. M. Fink, P. J. Leek, G. Puebla, L. Steffen, and A. Wallraff, *Coplanar waveguide resonators for circuit quantum electrodynamics*, Journal of Applied Physics, 104:113904 (2008).

[6] Micro-Coax, *UT-085C-AL-TP-LL*, http://www.micro-coax.com/products/product-details/?type=alumiline&part_id=75 (25.2.2014).

[7] Penn Engineering, *Waveguide Sizes and Data*, http://www.pennengineering.com/waveguide.php (30.9.2013).

[8] David M. Pozar, *Microwave Engineering*, Fourth Edition, John Wiley & Sons, Inc. (2012).

[9] P-N Designs, *Waveguide Primer*, http://www.microwaves101.com/encyclopedia/waveguide.cfm (19.2.2014).

[10] G. Weihs, et al., *Violation of Bell's Inequality under Strict Einstein Locality Conditions*, Phys. Rev. Lett. 81, 23, 5039 (1998).

Eidgenössische Technische Hochschule Zürich
Swiss Federal Institute of Technology Zurich

Declaration of originality

The signed declaration of originality is a component of every semester paper, Bachelor's thesis, Master's thesis and any other degree paper undertaken during the course of studies, including the respective electronic versions.

Lecturers may also require a declaration of originality for other written papers compiled for their courses.

I hereby confirm that I am the sole author of the written work here enclosed and that I have compiled it in my own words. Parts excepted are corrections of form and content by the supervisor.

Title of work (in block letters):

Simulation and characterization of waveguides and the coupling to 3D microwave cavities

Authored by (in block letters):
For papers written by groups the names of all authors are required.

Name(s):	**First name(s):**
Ruffieux	Silvia

With my signature I confirm that

- I have committed none of the forms of plagiarism described in the 'Citation etiquette' information sheet.
- I have documented all methods, data and processes truthfully.
- I have not manipulated any data.
- I have mentioned all persons who were significant facilitators of the work.

I am aware that the work may be screened electronically for plagiarism.

Place, date	**Signature(s)**
Zürich, 8. April 2014	S. Ruffieux

For papers written by groups the names of all authors are required. Their signatures collectively guarantee the entire content of the written paper.